Third-Order Nonlinear Optical Properties of Some Electron-Rich Iron Mono- and Trinuclear Alkynyl Complexes

Marie P. Cifuentes,[†] Mark G. Humphrey,*[,†] Joseph P. Morrall,[†,‡] Marek Samoc,[‡] Frédéric Paul,*[,§] Claude Lapinte,[§] and Thierry Roisnel[⊥]

Department of Chemistry, Australian National University, Canberra, ACT 0200, Australia, Laser Physics Centre, Research School of Physical Sciences and Engineering, Australian National University, Canberra, ACT 0200, Australia, Organométalliques et Catalyse: Chimie et Electrochimie Moléculaire, UMR CNRS 6509, Institut de Chimie de Rennes, Université de Rennes 1, Campus de Beaulieu, 35042 Rennes Cedex, France, and Laboratoire de Chimie du Solide et Inorganique Moléculaire, UMR CNRS 6511, Institut de Chimie de Rennes, Université de Rennes 1, Campus de Beaulieu, 35042 Rennes Cedex, France

Received January 13, 2005

The syntheses of [1,3,5-{(η^2-dppe)(η^5-C_5Me_5)FeC≡C-4-C_6H_4C≡C}$_3C_6H_3$] (**1**) and [(η^2-dppe)-(η^5-C_5Me_5)Fe(C≡C-1,4-C_6H_4C≡CPh)] (**2**) are reported, together with an X-ray diffraction study of **2**. The linear optical spectra of these compounds reveal characteristic low-energy transitions at 430 and 436 nm, respectively, significantly red shifted in comparison to those recorded for [1,3,5-{(η^2-dppe)(η^5-C_5Me_5)FeC≡C}$_3C_6H_3$] (**3**) and [(η^2-dppe)(η^5-C_5Me_5)FeC≡CPh] (**4**), respectively. Cubic nonlinear optical response data for **1**, **2**, and **4** are reported. Cubic molecular nonlinearities by Z-scan at 695 nm reveal an increase in nonlinearities upon introduction of the ligated metal unit and progression from linear monometallic complex to octupolar trimetallic complex. Oxidation of **1** to $\mathbf{1}^{3+}$ results in a change of sign and magnitude of the imaginary (absorptive) part of the third-order nonlinearity; that is, the molecule can be electrochemically cycled between two-photon absorber and saturable absorber states.

Introduction

Materials with optimized nonlinear optical (NLO) properties are required for the control and processing of signal-carrying light beams in the emerging photonics-based technologies.[1,2] Organometallic alkynyl complexes have considerable potential in this respect; electron-rich ligated metal centers used as powerful donor sites assembled around a central core by employing extended unsaturated carbon-rich linkers can afford complexes with significant second- and third-order nonlinearities.[3−8] In addition, when the metal centers are redox active, such assemblies afford the possibility of redox-based switching or modulation of the NLO properties.[7,9−12] Electrochromic switching of third-order NLO properties has recently been realized with mono- and trinuclear ruthenium alkynyl complexes by some of us.[1,2,13]

Iron alkynyl complexes of similar structures may possess more readily accessible oxidation potentials than their ruthenium analogues[14] and comparable NLO properties.[7,10,15,16] Investigation of the potential of several iron alkynyl complexes for electrochromic switching of the third-order NLO activity was therefore very appealing. We report herein the synthesis and characterization of the trinuclear iron alkynyl complex **1** and of the mononuclear model complex **2** of related structure (Chart 1), as well as an assessment of the potential of the former for electrochemically induced third-order

[†] Department of Chemistry, Australian National University.
[‡] Laser Physics Centre.
[§] Organométalliques et Catalyse: Chimie et Electrochimie Moléculaire.
[⊥] Laboratoire de Chimie du Solide et Inorganique Moléculaire.

(1) Cifuentes, M. P.; Powell, C. E.; Humphrey, M. G.; Heath, G. A.; Samoc, M.; Luther-Davies, B. *J. Phys. Chem. A* **2001**, *105*, 9625−9627.
(2) Samoc, M.; Luther-Davies, B.; Humphrey, M. G.; Cifuentes, M. P.; McDonagh, A. M.; Powell, C. E.; Heath, G. A. *SPIE Proc., Int. Soc. Opt. Eng.* **2001**, *4461*, 65−77.
(3) Whittall, I. R.; McDonagh, A. M.; Humphrey, M. G.; Samoc, M. *Adv. Organomet. Chem.* **1998**, *42*, 291−362.
(4) Whittall, I. R.; McDonagh, A. M.; Humphrey, M. G.; Samoc, M. *Adv. Organomet. Chem.* **1999**, *43*, 349−405.
(5) McDonagh, A. M.; Humphrey, M. G.; Samoc, M.; Luther-Davies, B. *Organometallics* **1999**, *18*, 5195−5197.
(6) McDonagh, A. M.; Humphrey, M. G.; Samoc, M.; Luther-Davies, B.; Houbrechts, S.; Wada, T.; Sasabe, H.; Persoons, A. *J. Am. Chem. Soc.* **1999**, *121*, 1405−1406.
(7) Weyland, T.; Ledoux, I.; Brasselet, S.; Zyss, J.; Lapinte, C. *Organometallics* **2000**, *19*, 5235−5237.
(8) Hurst, S. K.; Cifuentes, M. P.; McDonagh, A. M.; Humphrey, M. G.; Samoc, M.; Luther-Davies, B.; Asselberghs, I.; Persoons, A. *J. Organomet. Chem.* **2002**, *642*, 259−267.
(9) (a) Coe, B. J.; Houbrechts, S.; Asselberghs, I.; Persoons, A. *Angew. Chem., Int. Ed.* **1999**, *38*, 366−369. (b) Coe, B. J. *Chem. Eur. J.* **1999**, *5*, 2464−2471.
(10) Paul, F.; Costuas, K.; Ledoux, I.; Deveau, S.; Zyss, J.; Halet, J.-F.; Lapinte, C. *Organometallics* **2002**, *21*, 5229−5235.
(11) Malaun, M.; Reeves, Z. R.; Paul, R. L.; Jeffery, J. C.; McCleverty, J. A.; Ward, M. D.; Asselberghs, I.; Clays, K.; Persoons, A. *Chem. Commun.* **2001**, 49−50.
(12) Asselberghs, I.; Clays, K.; Persoons, A.; Ward, M. D.; McCleverty, J. A. *J. Mater. Chem.* **2004**, *14*, 2831−2839.
(13) Powell, C. E.; Humphrey, M. G.; Cifuentes, M. P.; Morrall, J. P.; Samoc, M.; Luther-Davies, B. *J. Phys. Chem. A* **2003**, *107*, 11264−11266.
(14) Paul, F.; Lapinte, C. *Coord. Chem. Rev.* **1998**, *178/180*, 427−505.
(15) Weyland, T.; Costuas, K.; Mari, A.; Halet, J.-F.; Lapinte, C. *Organometallics* **1998**, *17*, 5569−5579.
(16) Weyland, T.; Costuas, K.; Toupet, L.; Halet, J.-F.; Lapinte, C. *Organometallics* **2000**, *19*, 4228−4239.

10.1021/om050030g CCC: $30.25
Publication on Web 07/12/2005

Chart 1. Molecular Structures of 1−4

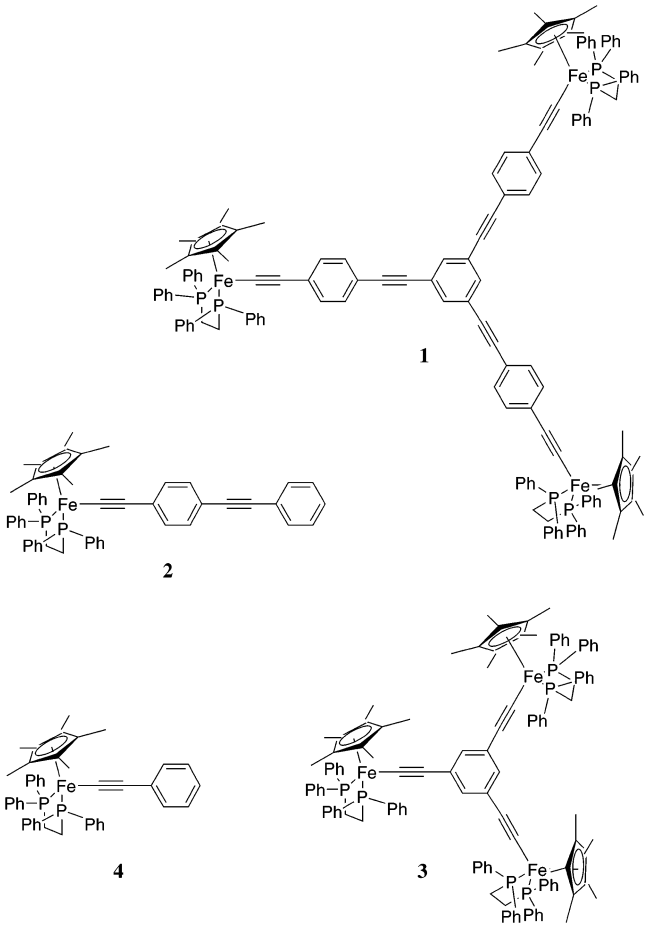

NLO switching. Relevant data on the previously reported trinuclear organoiron complex **3** and its mononuclear counterpart **4**[16−18] (Chart 1) are also included. This series of complexes affords the possibility of assessing the contribution of each branch of the C_{3v} trinuclear structure (when comparing **1** and **2**) and the influence of extending the organic bridge between the metal sites (when comparing **1** with **3**, or **2** with **4**).

Results and Discussion

Synthesis and Characterization of Alkynyl Complexes 1 and 2. The desired complexes were isolated from reactions between the precursor iron chloro complex and the organic alkynes. Activation of the terminal alkyne groups yielded the corresponding vinylidene complexes, and deprotonation of the latter formed the alkynyl complexes (Scheme 1). In each case, the intermediate vinylidene complexes **1′** and **2′** were isolated and purified before deprotonation. Recrystallization of the products **1** and **2** was also needed to isolate these compounds in a pure state because minute amounts of unidentified complexes were still present in the crude reaction mixture. The intermediate vinylidene complexes were not extensively characterized, their identity and purity being confirmed by infrared and ^{31}P and ^{1}H NMR spectroscopies. However, both alkynyl complexes **1** and **2** were fully characterized by LSIMS, cyclic voltammetry, and the usual spectroscopic techniques (Tables 1−3). The identity of complex **2** was confirmed by a single-crystal X-ray structural study (Tables 4 and 5).

The ^{1}H and ^{31}P NMR spectra are not unusual for such compounds and confirmed the purity of the isolated samples.[7,15,16,18] Thus, the ^{13}C NMR spectra exhibit the characteristic signatures of the alkynyl group at ca. 145 ppm for α-carbon atoms and at ca. 110 ppm for β-carbon atoms. The former are easily recognizable triplets due to their coupling to the phosphorus atoms of the 1,2-bis(diphenylphosphino)ethane (dppe) ligand.

Two absorptions are also observed in the infrared spectra $\nu_{C\equiv C}$ region for each of these compounds, one very strong in the usual range for iron alkynyls and a second, weaker, around 2200 cm^{-1} (Table 1). Although rather weak in **1** and barely detectable in **2**, a corresponding very weak absorption is also observed at quite similar wavenumbers in the infrared spectra of the organic alkyne precursors used to synthesize the complexes. Raman spectroscopy further suggests that these absorptions in **1** and **2** correspond to a fundamental mode rather than a combination mode or harmonic mode.[19]

Vibronic selection rules suggest that C_{3v} symmetric complexes such as **1** or **3** should possess two stretching modes (A_1 and E) in the infrared and Raman spectra for each set of equivalent alkyne bonds,[20] the A_1 mode being only weakly infrared-active.[21] Thus, four alkynyl stretching modes should be observed for **1**, two intense ones (E) and two weaker ones (A_1). We believe, however, that these vibronic fundamentals are not all distinct in the vibronic spectra and that the observed modes actually correspond to the two chemically nonequivalent alkyne bonds present in **1**. In accordance with this hypothesis, the two stretching fundamentals (A_1 and E) expected in the alkynyl region for the trinuclear analogue of **1** belonging to the same symmetry group and possessing only one alkynyl spacer (i.e., **3**) were previously not differentiated by infrared spectroscopy.[15] Raman spectroscopy reveals that only one absorption around 2047 cm^{-1} is present in the vibronic spectrum of **3** (a shoulder at 2051 cm^{-1} can nevertheless be detected which corresponds, perhaps, to the second expected mode).

This hypothesis also implies that the two absorptions detected in the $\nu_{C\equiv C}$ region for **2** correspond to the chemically nonequivalent alkyne groups. In accordance with this, two clearly distinct absorptions at 2140 (vw) and 2040 (s) cm^{-1} were detected for the *meta* analogue (**5**; Chart 2) of **2** (Table 1) and also for the mononuclear *para*-substituted complexes [(η^2-dppe)(η^5-C_5Me_5)Fe(C≡C-1,4-C_6H_4C≡CSiR_3)] **6a** (R = Me; 2146, 2038 cm^{-1}) and **6b** (R = ^{i}Pr; 2145, 2042 cm^{-1}), possessing two chemically nonequivalent alkynes (Chart 2).[22]

(17) Connelly, N. G.; Gamasa, M. P.; Gimeno, J.; Lapinte, C.; Lastra, E.; Maher, J. P.; Le Narvor, N.; Rieger, A. L.; Rieger, P. H. *J. Chem. Soc., Dalton Trans.* **1993**, 2575−2578.

(18) Denis, R.; Toupet, L.; Paul, F.; Lapinte, C. *Organometallics* **2000**, *19*, 4240−4251.

(19) Paul, F.; Mevellec, J.-Y.; Lapinte, C. *J. Chem. Soc., Dalton Trans.* **2002**, 1783−1790.

(20) Coat, F.; Paul, F.; Lapinte, C.; Toupet, L.; Costuas, K.; Halet, J.-F. *J. Organomet. Chem.* **2003**, *683*, 368−378.

(21) If spherically symmetric metallic end-groups are considered,[20] the symmetry group is now D_{3h} and the $\nu_{C\equiv C}$ fundamentals belong to the A_1' and E′ representations with A_1' modes inactive in the infrared.

(22) Courmarcel, J.; Le Gland, G.; Toupet, L.; Paul, F.; Lapinte, C. *J. Organomet. Chem.* **2003**, *670*, 108−122.

Scheme 1. Syntheses of 1 and 2

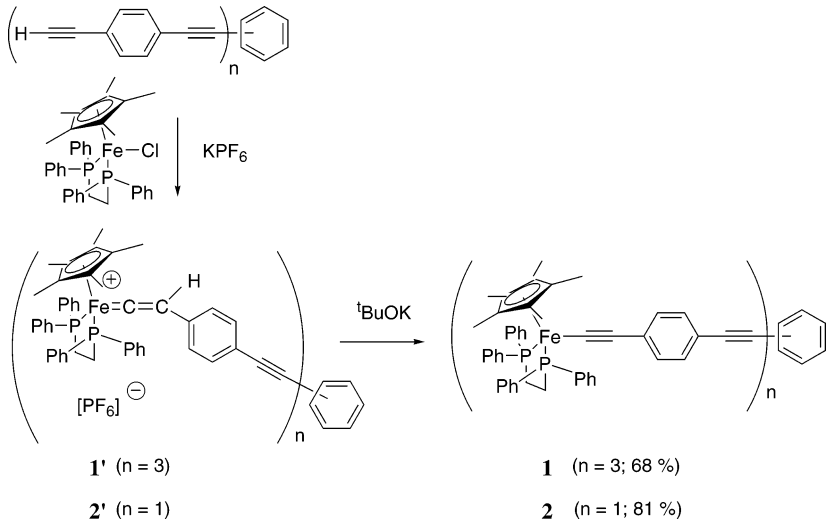

Table 1. Infrared Data for Selected Complexes in CH_2Cl_2 Solution[a] (cm^{-1})

compound	Fe(II) $\nu_{C\equiv C}$	Fe(III) $\nu_{C\equiv C}$	$\Delta\nu_{C\equiv C}$[b]	ref
[{[Fe]C≡C-4-C_6H_4C≡C}$_3C_6H_3$] (**1**)	2202	not obsd		this work
	2046	1995	−51	
[[Fe]C≡C-4-C_6H_4C≡CPh] (**2**)	2209	2213	+4	this work
	2044	1987	−57	
[{[Fe]C≡C}$_3C_6H_3$] (**3**)	2050	2010	−40	15
[[Fe]C≡CPh] (**4**)	2053	2021	−49[c]	18
		1988		
[[Fe]C≡C-3-C_6H_4C≡CPh] (**5**)	2134	not obsd		22
	2046			

[a] [Fe] ≡ (η^2-dppe)(η^5-C_5Me_5)Fe. Solid state $\nu_{C\equiv C}$ values obtained in KBr for isolated complexes are given in the Experimental Section. [b] Neutral vs oxidized $\nu_{C\equiv C}$ difference. [c] Mean difference: two bands were observed for the Fe(III) parent, presumably due to Fermi coupling.[19]

Table 2. Electrochemical Data for Selected Complexes[a]

compound	ΔE_p (V)	E_0 (V)[b]	i_c/i_a	ref
[{[Fe]C≡C-4-C_6H_4C≡C}$_3C_6H_3$] (**1**)	0.11	−0.15	1	this work
[[Fe]C≡C-4-C_6H_4C≡CPh] (**2**)	0.09	−0.13	1	this work
[{[Fe]C≡C}$_3C_6H_3$] (**3**)	0.07	−0.25	1	15
	0.06	−0.13	1	
	0.07	0.00	1	
		+0.53		
[[Fe]C≡CPh] (**4**)	0.08	−0.15	1	18
[[Fe]C≡C-3-C_6H_4C≡CPh] (**5**)	0.08	−0.13	1	22

[a] [Fe] ≡ (η^2-dppe)(η^5-C_5Me_5)Fe. All E values in V vs SCE. Conditions: CH_2Cl_2 solvent, 0.1 M (N^nBu_4)(PF_6) supporting electrolyte, 20 °C, Pt electrode, sweep rate 0.100 V s^{-1}. The ferrocene/ferrocenium (Fc/Fc^+) complex was used as an internal reference for potential measurements. [b] E_0 values corrected for Fc/Fc^+ at 0.460 V vs SCE in CH_2Cl_2, ΔE_p = 0.06 V. [33]

The absorption at ca. 2200 cm^{-1} in the spectra of **1** and **2** is rather energetic for an organic aryl-alkyne $\nu_{C\equiv C}$ band, especially so when compared to the corresponding $\nu_{C\equiv C}$ in **5** or in **6a**,**b**. These modes certainly benefit from strong vibronic coupling to other vibrators belonging to the same symmetry representation, possibly C−C stretching modes involving the nearby aromatic core and perhaps also (but to a smaller extent) C≡C stretching modes of the nearby iron-acetylide linkage. The iron-acetylide $\nu_{C\equiv C}$ wavenumbers are not significantly different from alkynyl stretching modes usually observed in related mononuclear iron(II) alkynyl complexes.[19]

As revealed by cyclic voltammetry (Table 2), complexes **1** and **2** undergo a reversible oxidation at similar potentials. The mononuclear complex **2** is slightly more difficult to oxidize than the unsubstituted mononuclear complex **4**. Its oxidation potential is similar to that previously reported for the *meta* analogue **5**,[22] consistent with the electron-withdrawing character of the 4-phenylalkynyl substituent.[23] Compound **2** is oxidized at a slightly more positive potential than **1**. The latter shows only one oxidation wave at −0.15 V vs SCE for the three iron-based oxidations, whereas **3** exhibits three distinct reversible redox processes. The redox wave of **1** is quite large (ΔE_p = 0.11 V) in comparison to the strictly monoelectronic process recorded for **2** (ΔE_p = 0.09 V) or for **3** (ΔE_p = 0.07 V), suggesting that the three oxidations of **1** do not actually take place at exactly the same potential. From a thermodynamic point of view, the data would indicate that the mixed-valence states $\mathbf{1}^+$ and $\mathbf{1}^{2+}$ have a slight extra stability. However, the cyclic voltammetry plainly shows that **1** cannot be unambiguously categorized as a class II mixed-valence complex in the classification of Robin and Day,[14,24,25] in contrast to **3**.[16]

The relatively low energy of the acetylide $\nu_{C\equiv C}$ in the infrared spectrum of **2** (and also in **1**) contrasts with the high energy of the other $\nu_{C\equiv C}$ corresponding to the organic alkyne (see above). If the existence of vibronic coupling is not considered, the observed wavenumber

(23) Costuas, K.; Paul, F.; Toupet, L.; Halet, J.-F.; Lapinte, C. *Organometallics* **2004**, *23*, 2053−2068.
(24) Robin, M. B.; Day, P. *Adv. Inorg. Chem. Radiochem.* **1967**, 247−422.
(25) Astruc, D. *Electron Transfer and Radical Processes in Transition-Metal Chemistry*; VCH Publishers: New York, 1995.

Table 3. UV−Vis Data for Selected Complexes in CH_2Cl_2[a]

compound	absorptions in nm ($10^{-3}\epsilon$ in M^{-1} cm^{-1})	ref
[{[Fe]C≡C-4-C_6H_4C≡C}$_3C_6H_3$] (**1**)	314 (91.5); 394 (sh, 40.4); 460 (62.2)	this work
[[Fe]C≡C-4-C_6H_4C≡CPh] (**2**)	394 (sh, 31.5); 298 (37.1); 436 (22.9)	this work
[{[Fe]C≡C}$_3C_6H_3$] (**3**)	283 (53.0); 351 (35.0)	7
[[Fe]C≡CPh] (**4**)	277 (sh, 14.5); 350 (13.6)	this work

[a] [Fe] ≡ (η^2-dppe)(η^5-C_5Me_5)Fe.

Table 4. Crystal Data, Data Collection, and Refinement Parameters for 2

	2·C_7H_8
formula	$C_{52}H_{48}P_2Fe_1$·C_7H_8
fw	820.72
temp (K)	293(2)
cryst syst	triclinic
space group	*P*1
a (Å)	12.077(5)
b (Å)	12.333(5)
c (Å)	17.469(5)
α (deg)	83.013(5)
β (deg)	79.834(5)
γ (deg)	61.504(5)
V(Å^3)	2248.7(15)
Z	2
D_{calcd} (g cm^{-3})	1.212
cryst size (mm)	0.45 × 0.42 × 0.03
F(000)	862
diffractometer	KappaCCD (Nonius)
radiation	Mo Kα
abs coeff (mm^{-1})	0.442
data collection: θ_{max} (deg), frames, Ω rotation (deg), seconds/frame	27.5, 152, 2.0, 120
θ range	1.88−27.45
h k l range	−15/15 −15/15 −22/22
no. of total reflns	30 565
no. of unique reflns	10 268
no. of obsd reflns [$I > 2\sigma(I)$]	7686
no. of restraints/params	0/541
$w = 1/[\sigma^2(F_o)^2 + (aP)^2+bP]$ (where $P = [F_o^2 + F_c^2]/3$)	$a = 0.0673$ $b = 0.7862$
final *R*	0.0477
R_w	0.1245
R indices (all data)	0.0704
R_w (all data)	0.1409
goodness of fit/F^2 (S_w)	1.017
$\Delta\rho_{max}$ (e Å^{-3})	0.314
$\Delta\rho_{min}$ (e Å^{-3})	−0.466

Table 5. Selected Bond Lengths (Å) and Angles (deg) for 2

	2·C_7H_8
Selected Bond Lengths	
Fe−$(Cp^*)_{centroid}$	1.738
Fe−P1	2.1906(10)
Fe−P2	2.1805(10)
Fe−C37	1.893(4)
C37−C38	1.218(3)
C38−C39	1.434(3)
C39−C40	1.396(4)
C40−C41	1.376(4)
C41−C42	1.384(4)
C42−C43	1.392(4)
C43−C44	1.384(4)
C42−C45	1.441(3)
C45−C46	1.186(4)
C46−C47	1.431(4)
Selected Bond Angles	
P1−Fe−P2	86.26(4)
P1−Fe−C37	86.99(7)
P2−Fe−C37	82.23(7)
Fe−C37−C38	178.7(2)
C37−C38−C39	173.9(3)
C39−C40−C41	121.0(3)
C40−C41−C42	121.5(3)
C41−C42−C43	120.1(3)
C42−C45−C46	177.4(3)
C45−C46−C47	179.7(3)
Fe−$(Cp^*)_{centroid}$/C39−C40[a]	110.2
C42−C41/C47−C48[a]	3.5

[a] Dihedral angle (Cp* = pentamethylcyclopentadienyl ligand).

Chart 2. Molecular Structures of 5 and 6a,b

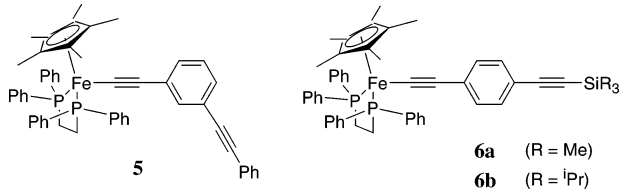

5 **6a** (R = Me) **6b** (R = ^{i}Pr)

would indicate a strong electron-withdrawing effect of the *para* "C≡C−Ar" substituent on the (η^2-dppe)(η^5-C_5Me_5)FeC≡C-1,4-C_6H_4− fragment, especially when compared to that previously observed for the mononuclear complex **4**. Indeed, the value is close to that observed for a C≡N substituent.[19] However, the electrochemical data tend to indicate a more moderate electron-withdrawing influence of the "C≡C-1,4-(C_6H_4)-C≡C−Ar" ligand, suggesting also the involvement of specific vibronic coupling in the above-mentioned acetylide $\nu_{C\equiv C}$. Within experimental accuracy, the redox potential found for **2** is similar to that previously reported for the *meta* analogue **5**,[22] indicating a mostly inductive electronic effect of the C≡CPh substituent. The trinuclear complex **1** is oxidized at a potential 0.02 V more negative than **2**, affording evidence that the electron-withdrawing effect exerted by the C≡C-1,3-C_6H_3C≡C− spacer is compensated by the presence of the electron-rich metal centers capping each branch of **1**. Not surprisingly, the extended carbon-rich bridge in **1** transmits the electron-releasing character of each metal center less efficiently than in the related complex **3**, which possesses a simple alkynyl bridge between the capping metal atoms and the central aryl ring. Thus, in **3**, the oxidation of the first metallic end-group occurs at a much more negative potential (−0.25 V vs SCE) and in a stepwise fashion.

In the visible range, the electronic spectra of **1** and **2** present one distinct low-energy band (Table 3), which corresponds to a MLCT transition, analogous to **3** and **4**, which possess shorter alkynyl ligands. As expected, this electronic transition is bathochromically shifted by 109 or 86 nm in proceeding from **3** to **1** or **4** to **2**, respectively, consistent with the extension of conjugation. While progression from mononuclear to trinuclear structure has apparently no influence on the MLCT in **3** and **4**, this change results in a slight bathochromic shift of ca. 25 nm in proceeding from **2** to **1** (Figure 1). The extinction coefficient for this absorption in **1** is roughly three times that observed for **2**, in accordance with a compound possessing three iron-based chromophores.

X-ray structure of [(η^2-dppe)(η^5-C_5Me_5)Fe(C≡C-1,4-C_6H_4C≡CPh)] (2). The mononuclear complex **2** crystallizes in the triclinic space group. The crystal-

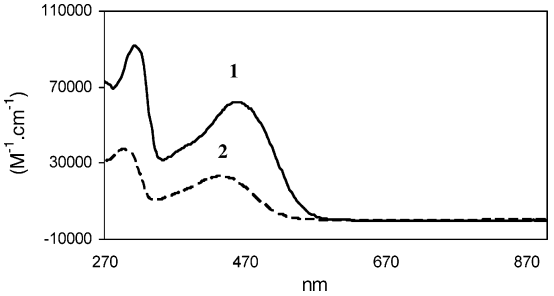

Figure 1. UV−vis spectra of **1** and **2**.

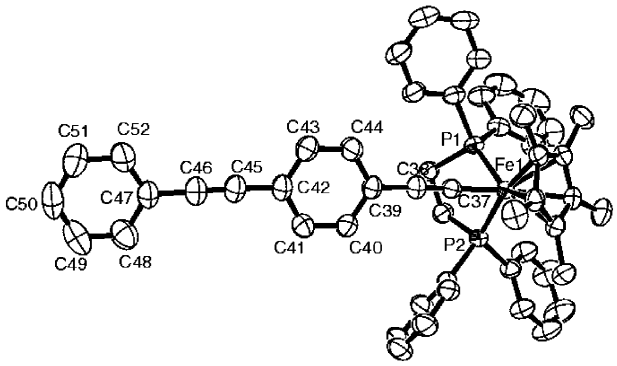

Figure 2. Thermal ellipsoid plot of **2**. Thermal ellipsoids are at the 50% probability level. Hydrogen atoms have been omitted for clarity.

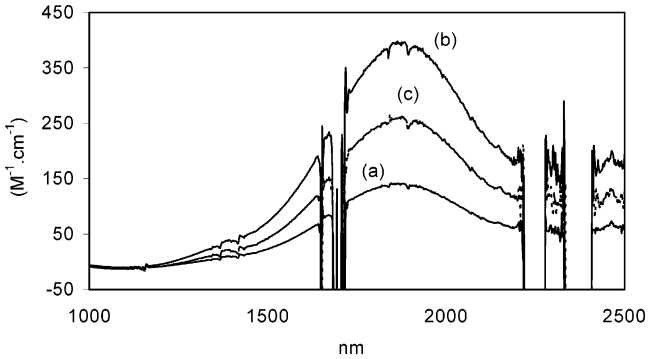

Figure 3. NIR spectra of $\mathbf{2}^{+}$ (a), $\mathbf{1}^{3+}$ (b), and a mixture of **1**, $\mathbf{1}^{+}$, $\mathbf{1}^{2+}$, and $\mathbf{1}^{3+}$ (c).

lographic data (Tables 4 and 5) are not unusual in terms of bond lengths, conformation, and angles for such mononuclear piano-stool iron compounds.[18,23] The Fe−C bond (1.89 ± 0.01 Å) and the C≡C bond (1.22 ± 0.01 Å) resemble those observed for the [(η^2-dppe)(η^5-C_5Me_5)-Fe(C≡CPh)] complex **4** (1.89 ± 0.01 and 1.20 ± 0.01 Å, respectively). A slight bending along the Fe−C≡C−aryl axis, usually observed with complexes possessing electron-withdrawing substituents on the aryl ring,[18] is also observed here, although the overall bending/conformation of the carbon-rich ligand is presumably induced by packing forces.[26]

Brief Spectroscopic Characterization of the Oxidized States $\mathbf{1}^{3+}$ and $\mathbf{2}^{+}$. The stability and electronic structure of the oxidized complexes $\mathbf{1}^{+}$, $\mathbf{1}^{2+}$, $\mathbf{1}^{3+}$, and $\mathbf{2}^{+}$ were briefly investigated by infrared, electron spin resonance (ESR), near-infrared (NIR), and UV−vis−NIR spectroscopies; particular attention was paid to the absorptions of these redox states in the NIR domain, since resonant absorption of the laser beam employed for the NLO studies described below could typically take place in this frequency range.[1,2,27]

The oxidized complexes were generated in situ from the neutral precursors **1** and **2** in the IR, ESR, and NIR spectroscopic cells, using ferricinium hexafluorophosphate (Scheme 2). Oxidation is evidenced by a characteristic color change from orange to green (**1**) or brown (**2**). Completion of the reaction was confirmed by infrared spectroscopy, as described below. Ferricinium hexafluorophosphate, as well as the coproduced ferrocene, are silent in the various frequency domains explored. Because of the weak thermodynamic stability of the mixed-valent states $\mathbf{1}^{+}$ and $\mathbf{1}^{2+}$ revealed by cyclic voltammetry (see above), these compounds cannot be generated in situ in a pure state (i.e., the comproportionation constants are small). These compounds were therefore studied only in the NIR domain in equilibrium with various amounts of **1** and $\mathbf{1}^{3+}$. In contrast, the fully oxidized complexes $\mathbf{1}^{3+}$ and $\mathbf{2}^{+}$ can be quantitatively generated in situ using an excess of ferricinium salt.

Upon addition of the ferricinium oxidant, the characteristic $\nu_{C\equiv C}$ of the Fe(II) alkynyl group disappeared and a new absorption appeared at lower wavenumbers corresponding to the $\nu_{C\equiv C}$ of the Fe(III) complex cations (Table 1).[18,19] The acetylide $\nu_{C\equiv C}$ bands of $\mathbf{1}^{3+}$ and $\mathbf{2}^{+}$ reveal a slightly more pronounced decrease in bond order than is observed between **3** and $\mathbf{3}^{3+}$ or **4** and $\mathbf{4}^{+}$, suggestive of a stronger delocalization of the positive charge in the C≡C-1,4-C_6H_4C≡C− bridges relative to single C≡C bridges. Given the possible existence of large vibronic coupling involving the inner organic alkyne in **1** and **2** (see above), comparison of the infrared data with the values obtained for $\mathbf{3}/\mathbf{3}^{3+}$ and $\mathbf{4}/\mathbf{4}^{+}$ should be made cautiously. The formation of radicals is also indicated by characteristic ESR signals in frozen dichloromethane/1,2-dichloroethane glasses at 80 K.[17,28] These ESR signals are only apparent at low temperatures, consistent with their organometallic nature (Table 6). Thus, for $\mathbf{1}^{3+}$, as expected for an electron-rich polyradical species, a very broad signal is obtained at $g = 2.10$, similar to the one obtained previously for $\mathbf{3}^{3+}$.[15] Likewise, for $\mathbf{2}^{+}$, an anisotropic ESR signal exhibiting three g tensors reveals the presence of an iron-centered radical.[28]

No absorptions were detected for the pure Fe(II) alkynyl complexes **1** and **2** in the NIR domain, but very weak absorptions appeared upon addition of the ferricinium oxidant (Table 7 and Figure 3). Thus, a weak NIR absorption was observed near 1866 nm for **2** in the presence of (excess) ferricinium, this absorption most probably corresponding to a forbidden d−d transition in the Fe(III) cationic radical species $\mathbf{2}^{+}$.[28,29] Progressive addition of ferricinium oxidant was also performed on **1** (Figure 3). Under such conditions, the mixed-valent complexes $\mathbf{1}^{+}$ and $\mathbf{1}^{2+}$ are transiently generated upon partial oxidation. However, as mentioned previously, these mixed-valent complexes afford no significant extra stability, and as a consequence, a near-statistical mix-

(26) Szafert, S.; Gladysz, J. A. *Chem. Rev.* **2003**, *103*, 4175−4250.

(27) Powell, C. E.; Cifuentes, M. P.; Morrall, J. P.; Stranger, R.; Humphrey, M. G.; Samoc, M.; Luther-Davies, B.; Heath, G. A. *J. Am. Chem. Soc.* **2003**, *125*, 602−610.

(28) Paul, F.; Lapinte, C. Work in progress.

(29) Le Stang, S.; Paul, F.; Lapinte, C. *Inorg. Chim. Acta* **1999**, *291*, 403−425.

Scheme 2. Synthesis of 1^{m+} and 2^{+}

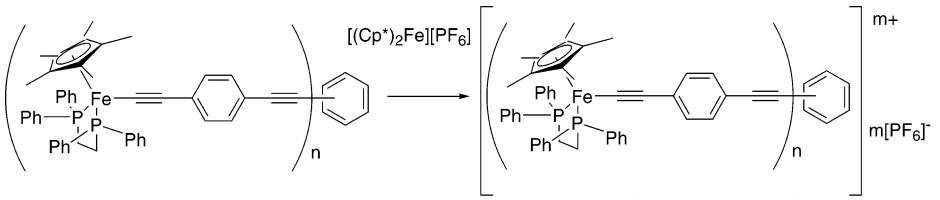

1 (n = 3) $\mathbf{1}^{m+}$ (n = 3; m = 1, 2, 3)

2 (n = 1) **2** (n = 1; m = 1)

Table 6. ESR Spectral Data for Compounds in Frozen CH_2Cl_2/1,2-$C_2H_4Cl_2$ Solutions at 80 K[a]

compound	g_1	g_2	g_3	Δg	ref
$[\{[Fe]C{\equiv}C\text{-}4\text{-}C_6H_4C{\equiv}C\}_3C_6H_3]^{3+}$ ($\mathbf{1}^{3+}$)		2.10 (ΔH_{pp} ca. 380 G)			this work
$[[Fe]C{\equiv}C\text{-}4\text{-}C_6H_4C{\equiv}CPh]^{+}$ ($\mathbf{2}^{+}$)	2.469	2.030	1.977	0.492	this work
$[\{[Fe]C{\equiv}C\}_3C_6H_3]^{3+}$ ($\mathbf{3}^{3+}$)		2.13[b] (ΔH_{pp} = 330 G)			15
$[[Fe]C{\equiv}CPh]^{+}$ ($\mathbf{4}^{+}$)	2.460	2.033	1.975	0.485	28, 45

[a] [Fe] ≡ (η^2-dppe)(η^5-C_5Me_5)Fe. At 77 or 80 K in CH_2Cl_2−$C_2H_4Cl_2$ (1:1) glass. [b] Broad single signal with small signals at g = 4.46 and 7.97.

Table 7. NIR Spectral Data for $\mathbf{1}^{3+}$, $\mathbf{2}^{+}$, $\mathbf{3}^{3+}$, and $\mathbf{4}^{+}$ in CH_2Cl_2 Solutions[a]

compound	ν_{max} in nm/cm^{-1} (ϵ in M^{-1} cm^{-1})	ref
$[\{[Fe]C{\equiv}C\text{-}4\text{-}C_6H_4C{\equiv}C\}_3C_6H_3]^{3+}$ ($\mathbf{1}^{3+}$)	1864/5364 (398)	this work
$[[Fe]C{\equiv}C\text{-}4\text{-}C_6H_4C{\equiv}CPh]^{+}$ ($\mathbf{2}^{+}$)	1866/5359 (145)	this work
$[\{[Fe]C{\equiv}C\}_3C_6H_3]^{3+}$ ($\mathbf{3}^{3+}$)	1851/5400 (ca. 150)	7
$[[Fe]C{\equiv}CPh]^{+}$ ($\mathbf{4}$+)	1846/5417 (94)	7, 28

[a] [Fe] ≡ (η^2-dppe)(η^5-C_5Me_5)Fe.

ture of the various redox isomers **1**, $\mathbf{1}^{+}$, $\mathbf{1}^{2+}$, and $\mathbf{1}^{3+}$ results when less than a 3-fold excess of ferricinium is present. The initial solution turned from orange to brown and finally to green. Again, an absorption centered at 1864 nm (i.e., very close to that recorded for $\mathbf{2}^{+}$) was detected and grew continuously. We also attribute this absorption to an Fe(III)-centered forbidden d−d transition. Its energy is apparently not very different in $\mathbf{1}^{+}$, $\mathbf{1}^{2+}$, and $\mathbf{1}^{3+}$, since its maximum does not appear to shift with increasing amounts of ferricinium. In accordance with our assignment of this band as arising from a metal-centered transition is the fact that the extinction coefficient for $\mathbf{1}^{3+}$ is roughly 3-fold that recorded for $\mathbf{2}^{+}$, as previously observed with the MLCT band in **1** and **2**. Importantly, no additional absorption corresponding to intervalence charge transfer (IVCT) transitions in the mixed-valent states $\mathbf{1}^{+}$ and $\mathbf{1}^{2+}$ was observed when less than 3 equiv of oxidant was present (trace c; Figure 3). The low comproportionation constants for $\mathbf{1}^{+}$ and $\mathbf{1}^{2+}$ and the fact that the corresponding IVCT bands might possibly be very weak render their detection particularly difficult under such conditions. Thus, we cannot at present exclude the possibility that weak IVCT bands are hidden by the band at 1864 nm. This experiment confirms, nevertheless, that $\mathbf{1}^{+}$ and $\mathbf{1}^{2+}$ are at best weakly coupled mixed-valent complexes.

The electrochromic behavior of **1** and **2** (Figure 4, Table 8) is broadly similar, consistent with their similar coordination spheres. Both **1** and **2** are transparent at frequencies below 17000 cm^{-1}, whereas oxidation to afford $\mathbf{1}^{3+}$ and $\mathbf{2}^{+}$ results in the appearance of strong absorption bands centered at ca. 13 700 cm^{-1}; oxidation therefore effectively "switches on" a transition at a wavelength accessible to our laser. Because a change in linear optical properties can be accompanied by a change in nonlinear properties, we examined $\mathbf{1}/\mathbf{1}^{3+}$ for the possibility of electrochemical switching of cubic nonlinearity (see below).

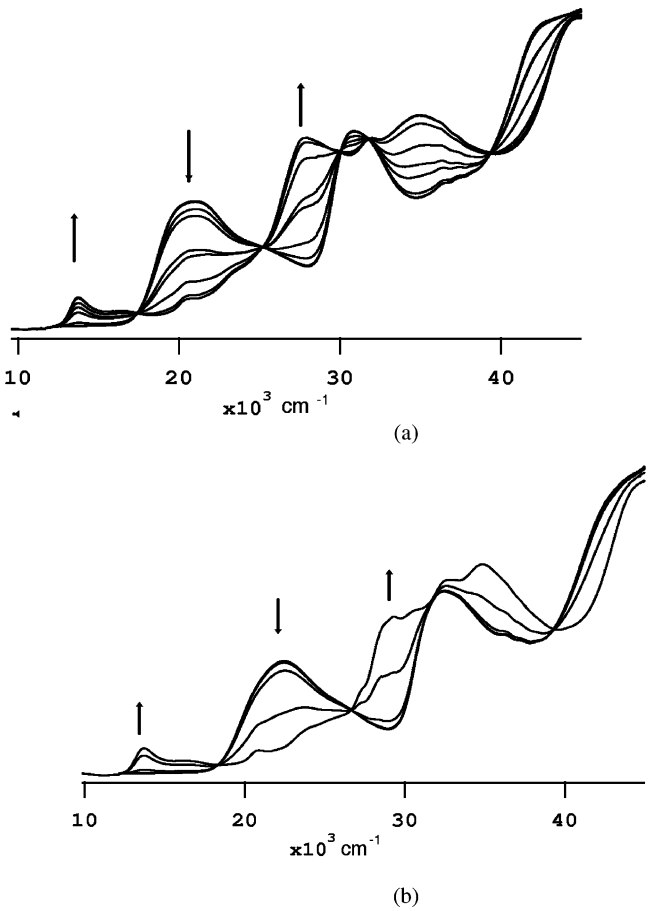

Figure 4. UV−vis−NIR spectra of CH_2Cl_2 solutions of (a) **1** and (b) **2** on application of 0.2 V (Fc/Fc^{+} = 0.56 V), in an OTTLE cell, path length 0.5 mm, during oxidation at 248 K.

Third-Order NLO Studies. Third-order nonlinearities of complexes **1**, **2**, and **4** were determined by Z-scan measurements at 695 nm and are listed in Table 9 (complex **3** was insufficiently soluble to measure its nonlinearity). The cubic nonlinearity at 800 nm of the precursor acetylene HC≡C-1,4-C_6H_4C≡CPh has been reported previously (γ_{real} = (25 ± 10) × 10^{-36} esu, γ_{imag}

Table 8. Spectroelectrochemical Data for 1 and 2

1		$\mathbf{1}^{3+}$	
λ_{max}, cm^{-1}	ϵ 10^4 M^{-1} cm^{-1}	λ_{max}, cm^{-1}	ϵ 10^4 M^{-1} cm^{-1}
21 470	5.4	13 790	1.9
25 450 sh	3.8	16 290 sh	1.2
31 580	8.3	20 640	2.0
		27 960	9.8
		31 870	10.8
		34 960	11.0
2		$\mathbf{2}^{+}$	
λ_{max}, cm^{-1}	ϵ 10^4 M^{-1} cm^{-1}	λ_{max}, cm^{-1}	ϵ 10^4 M^{-1} cm^{-1}
22 480	2.4	13 720	0.59
26 190	1.4	16 380	0.32
32 460	3.9	21 030	0.55
		24 030 sh	1.1
		29 360	3.5
		30 728	3.6
		32 620	4.3
		34 860	4.6

$< 6 \times 10^{-36}$ esu);[30] introduction of ligated iron centers in proceeding to **2** results in a 2-orders-of-magnitude increase in nonlinearity. The cubic nonlinearity of **4** had not been determined previously; it is low, but introduction of a phenylethynyl "spacer" in proceeding from **4** to **2** results in a dramatic increase in nonlinearity. Progression from the linear complex **2** to the octupolar complex **1** results in a further increase in nonlinearity, mirroring results obtained with the same alkynyl ligands in the bis{bis(diphenylphosphino)ethane}phenylethynylruthenium system.[6] Table 9 also includes two-photon absorption (TPA) cross-sections, σ_2 [TPA is an NLO process related to the imaginary component of the third-order nonlinearity; TPA materials have attracted significant recent interest for applications in multiphoton microscopy, optical limiting, and optical data storage]. We have previously noted significant TPA cross-sections in alkynylmetal complexes of octupolar composition,[1,5,31,32] and this is also true for **1**.

The cyclic voltammetry studies revealed that these complexes undergo reversible oxidation in solution, and UV−vis−NIR spectroelectrochemistry studies showed that these oxidation processes "switched on" optical transitions at long wavelength. Linear electrochromic effects should be accompanied by modifications in the NLO properties, an effect we have exploited to demonstrate NLO switching with related alkynylruthenium complexes.[1,13,27] In the present studies, we examined **1** in an OTTLE cell with switching potentials of 0.2 and −0.5 V (vs Ag/AgCl). Figure 5 shows closed-aperture Z-scans for the resting and oxidized forms of **1**. The as-prepared solution is a strong two-photon absorber, whereas the oxidized form loses this property and becomes a saturable absorber. At the same time, in all cases the refractive part of the hyperpolarizability is negative. Figure 6 illustrates the changes of linear transmission and nonlinear transmission occurring during the switching cycles. It is seen that the electrochemical changes are reversible. The calculated nonlinear properties of $\mathbf{1}^{3+}$ are given in Table 9.

Conclusion

New iron(II) alkynyl complexes **1** and **2** have been synthesized and characterized; their spectroscopic properties, in the light of other data collected for electron-rich iron alkynyl complexes,[23] have afforded some insight into their electronic structures. A brief spectroscopic investigation revealed that the oxidized Fe(III) species $\mathbf{1}^{3+}$ and $\mathbf{2}^{+}$ can be cleanly generated in situ by chemical oxidation and that these species are fairly stable radical cations, as expected from previous investigations on related species.[15,17,18]

Cubic nonlinearities for **1**, **2**, and **4** have been determined at 695 nm and are similar in magnitude to previously reported *trans*-[(η^2-dppe)$_2$Ru(C≡CPh)]-containing analogues. The structure−NLO property correlations in the ruthenium system are also seen in the present iron series: introduction of the ligated metal center increases nonlinearity, and there is a further significant increase in proceeding from linear monometallic complex to octupolar trimetallic complex. Spectroelectrochemical studies in the UV−vis−NIR domain revealed that oxidation "switches on" an absorption band with appreciable intensity, in a spectroscopic region that is transparent for the complexes in the resting state. The reversible $Fe^{II/III}$ couples in **1** have been exploited in an examination of NLO properties in the resting and oxidized forms. Similar to the ruthenium system, oxidation of **1** results in a change in sign and magnitude of γ_{imag} and σ_2, corresponding to cycling between a two-photon absorber and a saturable absorber. However, in contrast to our observations with the related ruthenium-containing complex, the redox cycling of **1** does not result in a change in sign of γ_{real}, a negative sign of the refractive nonlinearity being maintained.

Experimental Section

General Data. All manipulations were carried out under an inert atmosphere. Solvents or reagents were used as follows: Et_2O and *n*-pentane, distilled from Na/benzophenone; CH_2Cl_2, distilled from CaH_2 and purged with argon; NH^iPr_2, distilled from KOH and purged with argon; aryl bromides (Acros, >99%), opened/stored under Ar. [Fe(η^5-C_5H_5)$_2$][PF_6] was prepared by previously published procedures.[33] X-Band ESR spectra were recorded on a Bruker EMX-8/2.7 spectrometer. Transmittance-FTIR spectra were recorded using a Bruker IFS28 spectrometer (400−4000 cm^{-1}). Raman spectra of the solid samples were obtained by diffuse scattering on the same apparatus and recorded in the 100−3300 cm^{-1} range (Stokes emission) with a laser excitation source at 1064 nm, using a 1.05−1.06 μm laser source (15 mW) and a quartz separator with a FRA 106 detector. Liquid NIR spectra were recorded on a Cary 5 spectrometer. UV−visible spectra were recorded on an UVIKON XL spectrometer. Spectroelectrochemical data were recorded on a Cary 5 spectrophotometer (45 000−4000 cm^{-1}) in CH_2Cl_2. Solution spectra of the oxidized species at 253 K were obtained by electrogeneration (Thompson 401E potentiostat) at a Pt gauze working electrode within a cryostatted optically transparent thin-layer electrochemical (OTTLE) cell, path

(30) Hurst, S. K.; Cifuentes, M. P.; Morrall, J. P. L.; Lucas, N. T.; Whittall, I. R.; Humphrey, M. G.; Asselberghs, I.; Persoons, A.; Samoc, M.; Luther-Davies, B.; Willis, A. C. *Organometallics* **2001**, *20*, 4664−4675.

(31) Hurst, S. K.; Humphrey, M. G.; Isoshima, T.; Wostyn, K.; Asselberghs, I.; Clays, K.; Persoons, A.; Samoc, M.; Luther-Davies, B. *Organometallics* **2002**, *21*, 2024−2026.

(32) Hurst, S. K.; Lucas, N. T.; Humphrey, M. G.; Isoshima, T.; Wostyn, K.; Asselberghs, I.; Clays, K.; Persoons, A.; Samoc, M.; Luther-Davies, B. *Inorg. Chim. Acta* **2003**, *350*, 62−76.

(33) Connelly, N. G.; Geiger, W. E. *Chem. Rev.* **1996**, *96*, 877−910.

Table 9. Experimental Linear and Cubic Nonlinear Optical Response Parameters

compound	$\lambda_{max}{}^b$ (ϵ)^c	$\gamma_{real}{}^d$	$\gamma_{imag}{}^d$	$\lvert\gamma\rvert^d$	$\sigma_2{}^e$
1	460 (62 200)	−3300 ± 800	2800 ± 700	4300 ± 1100	920 ± 250
2	436 (22 900)	−1500 ± 1200	200 ± 40	1500 ± 1200	66 ± 15
3	351 (35 000)	*f*			
4	350 (13 600)	110 ± 100	17 ± 10	110 ± 100	5.6 ± 3
$\mathbf{1}^{3+}$	1864 (398)	−2000 ± 1000	−3300 ± 1000	3900 ± 1400	−1100 ± 330

[a] Conditions: measurements were carried out in thf; all complexes are optically transparent at 695 nm. γ values are referenced to the nonlinear refractive index of silica $n_2 = 3 \times 10^{-16}$ cm^2 W^{-1}. [b] nm. [c] M^{-1} cm^{-1}. [d] 10^{-36} esu. [e] 10^{-50} cm^4 s. [f] Insufficiently soluble.

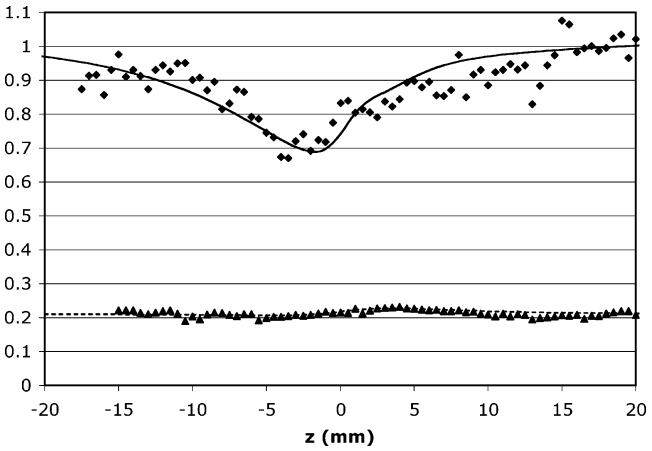

Figure 5. Closed aperture Z-scans for **1** (diamonds) and $\mathbf{1}^{3+}$ (triangles). The full line is the theoretical fit for a closed-aperture Z-scan dominated by two-photon absorption in the solute, and the dotted line is the fit for the closed-aperture scan dominated by absorption saturation.

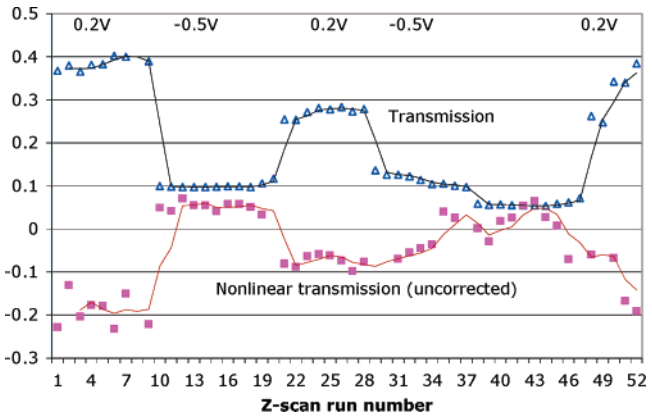

Figure 6. Changes of the linear transmission and the nonlinear transmission as determined from the relative depth (triangles: negative effect; nonlinear absorption) or height (squares: positive effect; nonlinear transmission) of the open-aperture Z-scan curve measured in-situ in an OTTLE cell when the electrochemical potential was cycled between the values of 0.2 and −0.5 V.

length 0.5 mm, mounted within the spectrophotometer. The electrogeneration potential was ca. 300 mV beyond $E_{1/2}$ for each couple, to ensure complete electrolysis. The efficiency and reversibility of each step was tested by applying a sufficiently positive potential to reoxidize the product; stable isosbestic points were observed in the spectral progressions for all the transformations reported herein. ^{1}H and ^{31}P NMR spectra were obtained on Brüker AVANCE 200 (200 MHz) and AVANCE 500 (500 MHz) spectrometers. ^{1}H and ^{31}P NMR chemical shifts are reported in units of parts per million (ppm) relative to residual protiated solvent and H_3PO_4, respectively. Cyclic voltammograms were recorded using a PAR 263 in CH_2Cl_2 (0.1 M $[N^nBu_4]PF_6$) at 25 °C at a platinum electrode, using a SCE reference electrode and ferrocene as internal calibrant (0.460 V), unless otherwise noted.[33] LSI/ESI-MS analyses were effected at the "Centre Regional de Mesures Physiques de l'Ouest" (Rennes; CRMPO) on a high-resolution MS/MS ZabSpec TOF Micromass spectrometer (8 kV). Elemental analyses were performed at the Center for Microanalyses of the CNRS at Lyon-Solaise or the CRMPO. Single-crystal X-ray data collection was performed with a Nonius Kappa-CCD diffractometer (Centre de Diffractométrie, Université de Rennes).

4-Ethynylphenylethynylbenzene and (HC≡C-4-C_6H_4C≡C)$_3C_6H_3$ were synthesized as previously reported.[6]

[{(η^2-dppe)(η^5-C_5Me_5)FeC≡C-1,4-C_6H_4C≡C}$_3C_6H_3$] (1). {HC≡C-4-C_6H_4C≡C}$_3C_6H_3$ (0.165 g, 0.369 mmol) was stirred in a mixture of 5 mL of thf and 15 mL of methanol with [(η^2-dppe)(η^5-C_5Me_5)FeCl]·Et_2O (0.772 g, 1.100 mmol) and NH_4PF_6 (0.245 g, 1.500 mmol). An orange precipitate formed in the initially green reaction medium. This suspension was stirred 5 days at 25 °C. After evaporation of the reaction mixture to dryness the resultant brown solid was extracted with 10 mL of dichloromethane. Concentration of the extract to dryness, washing with *n*-pentane (2 × 10 mL), and drying in vacuo afforded a mixture containing predominantly the corresponding vinylidene complex [{(η^2-dppe)(η^5-C_5Me_5)FeC=CH-1,4-C_6H_4C≡C}$_3C_6H_3$](PF_6)$_3$ (**1′**) as an air-sensitive brown solid (ca. 0.860 g, ca. 85%). Selected data for [{(η^2-dppe)(η^5-C_5Me_5)FeC=CH-1,4-C_6H_4C≡C}$_3C_6H_3$](PF_6)$_3$: FT-IR (ν, KBr, cm^{-1}): 2039 (w, C≡C), 1619 (s, Fe=C=C). ^{31}P{^{1}H} NMR (δ, $(CD_3)_2CO$, 81 MHz): 87.0 (s, dppe); −143.0 (septuplet, $^1J_{PF}$ = 707 Hz, PF_6^-). ^{1}H NMR (δ, $CDCl_3$, 200 MHz) 7.70−7.50 (m, 63H, $H_{Ar/dppe}$); 7.31 (m, 12H$_{Ar}$); 7.16 (d,$^3J_{HH}$ = 8.0 Hz, 6H, H_{Ar}); 6.38 (d,$^3J_{HH}$ = 8.0 Hz, 6H, H_{Ar}); 5.18 (t, $^4J_{HP}$ = 4.4 Hz, 3H, C=C(Ar)*H*); 3.26 (m, 6H, CH_{2dppe}); 2.69 (m, 6H, CH_{2dppe}); 1.68 (s, 45H, $C_5(CH_3)_5$). After recrystallization from dichloromethane/diethyl ether mixtures, the vinylidene salt (800 mg, 0.302 mmol) was then stirred 2 h in thf in the presence of excess potassium *tert*-butoxide (0.183 g, 1.620 mmol). After evacuation of the solvent, extraction with toluene, concentration of the extract to dryness, and subsequent washings with *n*-pentane, a crude orange solid was isolated containing the desired complex [1,3,5-{(η^2-dppe)(η^5-C_5Me_5)FeC≡C-1,4-C_6H_4C≡C}$_3C_6H_3$] (**1**). Recrystallization from toluene/pentane mixtures afforded the compound in a pure state (0.540 g, 0.244 mmol, 80%). Total yield 68%.

Color: brown. Anal. Calcd for $C_{144}H_{132}P_6Fe_3$: C, 78.05; H, 6.00. Found: C, 78.39; H, 5.83. MS (positive ETOF, CH_2Cl_2): *m/z* 2215 (**1**$^+$, 6); 589 ([(dppe)(C_5Me_5)Fe]$^+$, 100). IR (ν, KBr/CH_2Cl_2, cm^{-1}): 2199/2202 (w, C≡C); 2043/2046 (vs, FeC≡C); Raman (ν, neat, cm^{-1}) 2203 (s, C≡C); 2046 (s, Fe−C≡C). ^{31}P{^{1}H} NMR (δ, $CDCl_3$, 81 MHz, ppm): 100.9 (s). ^{1}H NMR (δ, $CDCl_3$, 200 MHz): 7.90 (m, 12H, H_{Ar}); 7.60−6.80 (m, 69H, H_{Ar}); 6.85 (d, $^3J_{HH}$ = 7.2 Hz, 6H, H_{Ar}); 2.67 (m, 6H, CH_{2dppe}); 2.02 (m, 6H, CH_{2dppe}), 1.48 (s, 45H, $C_5(CH_3)_5$). ^{13}C NMR (δ, $CDCl_3$, 50 MHz, ppm): 147.0 (t, $^2J_{CP}$ = 39 Hz, Fe−*C*≡C); 139.7−127.0 (m, 8$C_{Ar/dppe}$ + 2 $C_{quat./Ar}$ + 4 *C*-H$_{Ar}$); 124.9 (s, $C_{quat./Ar}$); 121.3 (br s, Fe−C≡*C*); 116.3 (t, $^2J_{CH}$ = 8 Hz, $C_{quat./Ar}$); 92.2 (br s, C≡*C*); 88.6 (br s, *C*≡C); 88.3 (br s, $C_5(CH_3)_5$); 31.1 (m, CH_{2dppe}); 10.5 (q, $^1J_{CH}$ = 126 Hz, $C_5(CH_3)_5$). E_0 (ΔE_p, i_{pa}/i_{pc}): −0.15 V (0.11, 1) V vs SCE. UV−vis (CH_2Cl_2): λ_{max}(ϵ/10^3 M^{-1} cm^{-1}) 314 (91.5); 394 (sh, 40.4); 460 (62.2).

[(η^2-dppe)(η^5-C_5Me_5)Fe(C≡C-1,4-C_6H_4C≡CPh)] (2). 4-Ethynylphenylethynylbenzene (0.165 g, 0.817 mmol) was stirred in a mixture of 3 mL of thf and 7 mL of methanol with [(η^2-dppe)(η^5-C_5Me_5)FeCl]·Et_2O (0.475 g, 0.761 mmol) and NH_4PF_6 (0.165 g, 1.020 mmol). The initially green suspension was stirred 12 h at 25 °C, after which time an orange precipitate had formed in the reaction medium. After evaporation of the reaction mixture to dryness the resultant orange solid was extracted with 15 mL of dichloromethane. Concentration of the extract to dryness, washing with *n*-pentane (2 × 10 mL), and drying in vacuo quantitatively afforded the corresponding vinylidene complex [(η^2-dppe)(η^5-C_5Me_5)Fe(C=CH-1,4-C_6H_4C≡CPh)](PF_6) (**2′**) as an air-sensitive orange solid after recrystallization from dichloromethane/diethyl ether mixtures (ca. 0.650 g, 92%). Selected data for [(η^2-dppe)(η^5-C_5Me_5)Fe(C=CH-1,4-C_6H_4C≡CPh)](PF_6): FT-IR (ν, KBr, cm^{-1}): 1626 (s, Fe=C=C, C≡C not observed). $^{31}P\{^1H\}$ NMR (δ, $CDCl_3$, 81 MHz): 87.7 (s, dppe); −143.1 (septuplet, $^1J_{PF}$ = 713 Hz, PF_6^-). ^1H NMR (δ, $CDCl_3$, 200 MHz): 7.70−7.05 (m, 26H, $H_{Ar/dppe}$); 6.27 (d, $^3J_{HH}$ = 8.2 Hz, 2H, H_{Ar}); 5.07 (t, $^4J_{HP}$ = 4.6 Hz, 1H, C=C(Ar)*H*); 3.14 (m, 2H, CH_{2dppe}); 2.52 (m, 2H, CH_{2dppe}); 1.60 (s, 15H, $C_5(CH_3)_5$). This vinylidene salt (0.650 g, 0.680 mmol) was then stirred 2 h in thf in the presence of excess potassium *tert*-butoxide (0.115 g, 1.020 mmol). After evacuation of the solvent and extraction with toluene, concentration of the extract to dryness, and subsequent washings with *n*-pentane, the crude orange complex [(η^2-dppe)(η^5-C_5Me_5)Fe(C≡C-1,4-C_6H_4C≡CPh)] (**2**) was isolated (0.460 g, 0.583 mmol, 86%). The complex was purified by recrystallization from toluene/pentane mixtures. Total yield: 81%.

Color: brown. Anal. Calcd for $C_{52}H_{48}P_2Fe_1$: C, 78.99; H, 6.12. Found: C, 78.46; H, 6.39. MS (positive ETOF, CH_2Cl_2): *m/z* 790 ([(dppe)(C_5Me_5)Fe(C≡CC_6H_4C≡CPh)]$^+$, 100); 589 ([(dppe)(C_5Me_5)Fe]$^+$, 5). IR (ν, KBr/CH_2Cl_2, cm^{-1}): 2208/2209 (w, C≡C); 2046/2044 (vs, FeC≡C); Raman (ν, neat, cm^{-1}) 2209 (s, C≡C); 2043 (s, FeC≡C). $^{31}P\{^1H\}$ NMR (δ, $CDCl_3$, 81 MHz, ppm): 100.9 (s). ^1H NMR (δ, $CDCl_3$, 200 MHz): 7.92−7.20 (m, 26H, H_{Ar}); 6.86 (m, 2H, H_{Ar}); 2.68 (m, 2H, CH_{2dppe}); 2.04 (m, 2H, CH_{2dppe}); 1.50 (s, 15H, $C_5(CH_3)_5$). ^{13}C NMR (δ, $CDCl_3$, 125 MHz, ppm): 146.5 (t, $^2J_{CP}$ = 39 Hz, Fe−*C*≡C); 139.5−127.0 (m, 8$C_{Ar/dppe}$ + 2 $C_{quat./Ar}$ + 4 *C*-H_{Ar}); 124.5 (m, $^2J_{CH}$ = 7 Hz, $C_{quat./Ar}$); 121.4 (br s, Fe−C≡*C*); 118.5 (t, $^2J_{CH}$ = 9 Hz, $C_{quat./Ar}$); 91.4 (t, $^3J_{CH}$ = 5 Hz, C≡*C*); 89.7 (t, $^3J_{CH}$ = 5 Hz, *C*≡C); 88.3 (s, $C_5(CH_3)_5$); 31.3 (m, CH_{2dppe}); 10.5 (q, $^1J_{CH}$ = 126 Hz, $C_5(CH_3)_5$). E_0 (ΔE_p, i_{pa}/i_{pc}): −0.13 V (0.09, 1) V vs SCE. UV−vis (CH_2Cl_2): λ_{max}($\epsilon/10^3$ M^{-1} cm^{-1}) 298 (37.1); 394 (sh, 31.5); 436 (22.9).

Crystallography. Crystals of **2** were obtained by slow diffusion of *n*-pentane into a solution of the complex in toluene. Single-crystal data collection was performed at room temperature, with Mo Kα radiation (λ = 0.71073 Å). A crystal-to-detector distance of 25.0 mm was used, and data collection (determination and optimization of the detector and goniometer positions) was performed with the help of the COLLECT program[34] to measure Bragg reflections of the asymmetric triclinic basal unit cell until θ = 27.5°. A total of 152 frames were recorded, using $\Delta\omega$ = 2.0° rotation scans to fill the asymmetric unit cell (exposure time = 120 s deg^{-1}). A total of 30 573 reflections were indexed, Lorentz−polarization corrected, and then integrated in the triclinic symmetry ($P\bar{1}$ point group) by the DENZO program of the Kappa-CCD software package.[35] Numerical absorption corrections were performed using the multiscan procedure[36] included in the WinGX program suite.[37] Structure determination was performed with SIR97,[38] revealing all the non-hydrogen atoms. The SHELXL program[39] was used to refine the structure. Atomic scattering factors were taken from the literature.[40] ORTEP views of **2** were realized with PLATON98.[41]

NLO Measurements. Third-order nonlinear optical measurements of **1**, **2**, and **4** were performed with an amplified femtosecond laser system consisting of a Clark-MXR CPA-2001 Ti-sapphire regenerative amplifier pumping a Light Conversion TOPAS optical parametric amplifier providing tunable femtosecond pulses of light. All experiments described here were performed with the doubled signal from the OPA at 695 nm. The default system repetition rate of 1 kHz was reduced to 250 Hz to minimize possible problems with cumulative photochemical and thermal effects.[42,43] Z-scans were recorded with a laser beam passed through a set of pinholes to generate a central lobe of an Airy pattern as described in ref 44. The focused spot size was about 35 μm. The peak light intensity used in the measurements was kept below 100 GW cm^{-2}. A series of Z-scans was recorded for two or three different concentrations of each of **1**, **2**, and **4** in thf. These measurements were used to determine the real and imaginary parts of the cubic polarizabilities γ_{real} and γ_{imag}. The solution nonlinear parameters were obtained by numerical fitting of the closed and open aperture Z-scans and calibration against the nonlinear refractive index of fused silica taken to be $n_2 = 3 \times 10^{-16}$ cm^2 W^{-1}. The solute hyperpolarizabilities were then obtained by assuming linear dependences of solution nonlinearity on the solute concentration.

Electrochemical switching of the nonlinearity of $\mathbf{1}^{3+}$ was investigated in an optically transparent thin-layer electrochemical (OTTLE) cell[27] where the platinum working electrode contained a ca. 1 mm diameter hole through which the Z-scan measurements could be performed, in situ, during the application of suitable electrochemical potentials.

Acknowledgment. The CNRS and Australian Research Council (ARC) are thanked for financial support. This project is proudly supported by the International Science Linkages Programme established under the Australian Government's innovation statement, Backing Australia's Ability. M.G.H. is an ARC Australian Professorial Fellow, and M.P.C. is an ARC Australian Research Fellow. We thank J.-Y. Thépot for experimental assistance with the ESR measurements.

Supporting Information Available: Full details of the X-ray structure of **2** including tables of atomic positional parameters, bond distances and angles, and anisotropic and isotropic thermal displacement parameters. This material is available free of charge via the Internet at http://pubs.acs.org.

OM050030G

(34) *Kappa CCD Software*; B. V. Nonius: Delft, The Netherlands, 1999.
(35) Otwinowski, Z.; Minor, W. In *Methods in Enzymology*; Carter, C. W., Sweet, R. M., Eds.; Academic Press: London, 1997; Vol. 276, pp 307−326.
(36) Blessing, R. H. *Acta Crystallogr.* **1995**, *A51*, 33−38.
(37) Farrugia, L. J. *J. Appl. Crystallogr.* **1999**, *32*, 837−838.
(38) Altomare, A.; Burla, M. C.; Camalli, M.; Cascarano, G.; Giacovazzo, C.; Guagliardi, A.; Moliterni, A. G. G.; Polidori, G.; Spagna, R. *J. Appl. Crystallogr.* **1999**, *32*, 115−119.
(39) Sheldrick, G. M. *SHELX97−2. Program for the refinement of crystal structures*; University of Göttingen: Germany, 1997.
(40) *International Tables for X-ray Crystallography*; Kluwer Academic Publishers: Dordrecht, 1992; Vol. C.
(41) Spek, A. L. *PLATON. A Multipurpose Crystallographic Tool*; Utrecht University: Utrecht, The Netherlands, 1998.
(42) Kamada, K.; Matsunaga, K.; Yoshino, A.; Ohta, K. *J Opt. Soc. Am. B−Opt. Phys.* **2003**, *20*, 529−537.
(43) Samoc, M.; Samoc, A.; Luther-Davies, B.; Humphrey, M. G.; Wong, M.-S. *Opt. Mater.* **2003**, *21*, 485−488.
(44) Rhee, B. K.; Byun, J. S.; van Stryland, E. W. *J. Opt. Soc. Am. B* **1996**, *13*, 2720−2723.
(45) Le Stang, S.; Paul, F.; Lapinte, C. *Organometallics* **2000**, *19*, 1035−1043.